TRANSVERSE BUNCHED BEAM INSTABILITIES - THEORY

F.J. Sacherer, CERN, Geneva, Switzerland

Introduction and Summary

A glance at Figs. 1 and 2 shows some of the contortions that a single bunch can undergo as it progressively destroys itself. The instability is driven by the surrounding environment, which extracts energy from the longitudinal directed motion of the bunch and converts it into growing transverse oscillations. As pointed out by Pellegrini[1] and Sands[2], simple rigid-bunch motion is possible only in the exceptional case of zero machine chromaticity; otherwise there is always a phase-shift between head and tail of a bunch. While the original and still widely used theory of Courant and Sessler[3] is restricted to rigid-bunch motion driven by long-range wake forces, the more recent head-tail theory of Pellegrini and Sands is restricted to the opposite limit of short-range wakes that act only from head to tail of a bunch, and not from bunch to bunch or over many revolutions. In addition, it was developed mainly for the unrealistic hollow-bunch distribution (see Fig. 3).

This paper presents a unified approach for a parabolic bunch that includes both single-turn and multi-turn effects. The main ingredients are

i) oscillation modes
ii) transverse coupling impedance $Z_\perp(\omega)$
iii) stability criterion.

The derivations are given in other papers[4,5] and only the results are presented here. A companion paper[6] presents the recent experimental observations in the CERN PS and Booster.

Classification of modes

If all particles have the same betatron frequency $\omega_\beta = Q\omega_0$ and synchrotron frequency ω_s, and we ignore the transit time of the bunch past a fixed observer, the first few head-tail modes appear as in Fig. 1a. The difference signal from a position monitor has the form

$$\Delta\text{-signal} \propto p_m(t)e^{j2\pi kQ} , \qquad (1)$$

for the k^{th} revolution.

Usually both Q and the revolution frequency ω_0 depend on momentum, so ω_β varies as a particle moves around a synchrotron orbit. The important quantity is the betatron phase of a particle at each position along the bunch as compared with the phase of the synchronous particle. The total phase-shift χ between head and tail has contributions from the Q-variation, the ω_0 variation, plus the finite transit time. In fact, the last two contributions cancel, and we are left with

$$\chi = \frac{\xi}{\eta} Q\omega_0\tau_L \quad \text{(radians)} , \qquad (2)$$

where $\xi = (dQ/Q)/(dp/p)$ is the chromaticity, $\eta = \gamma_T^{-2} - \gamma^{-2}$, and τ_L is the bunch length in seconds. The difference signal has the form (Figs. 1b and 1c)

$$\Delta\text{-signal} \propto p_m(t)e^{j\omega_\xi t + j2\pi kQ} , \qquad (3)$$

where

$$\omega_\xi = \frac{\chi}{\tau_L} = \frac{\xi}{\eta} Q\omega_0 . \qquad (4)$$

Note that for the example shown in Fig. 1c, mode 2 has appreciable contre-of-mass motion and would leave a long-range resistive-wall wake whereas mode 0 would not.

For a parabolic bunch, the modes $p_m(t)$ are approximately sines and cosines as shown in Fig. 1, while for a hollow bunch they appear as in Fig. 3 with

$$p_m(t) = \frac{T_m(t/\tau_L)}{\pi\sqrt{1 - (t/\tau_L)^2}} , \qquad (5)$$

where T_m is a Chebychev polynomial.

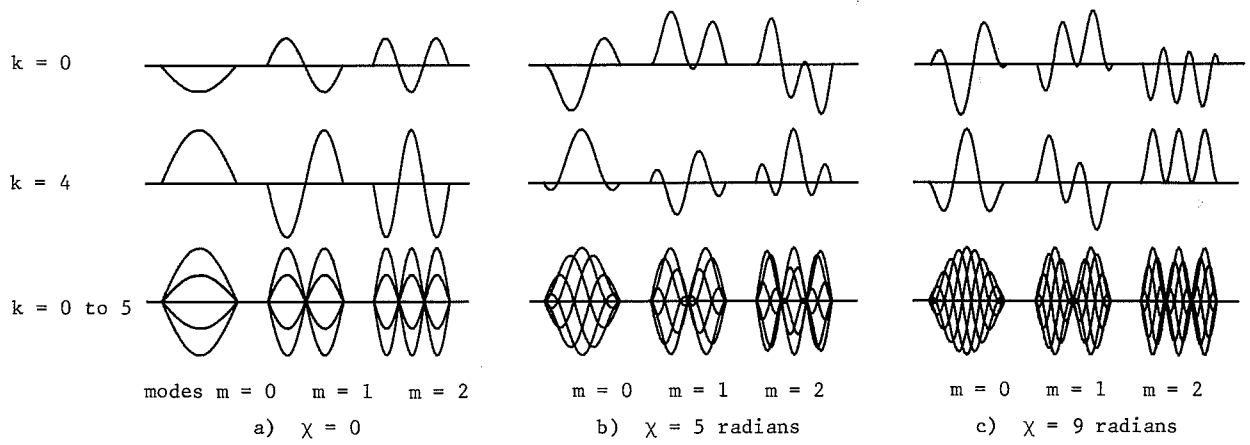

Fig. 1 Contortions of a single bunch on separate revolutions, and with six revolutions superimposed. Vertical axis is difference signal from position monitor, horizontal axis is time, and Q = 4.833.

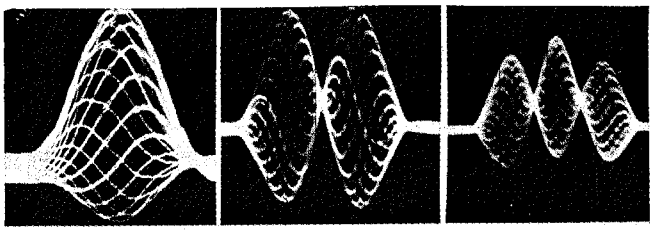

Fig. 2 Head-tail modes observed in the CERN Booster[6].

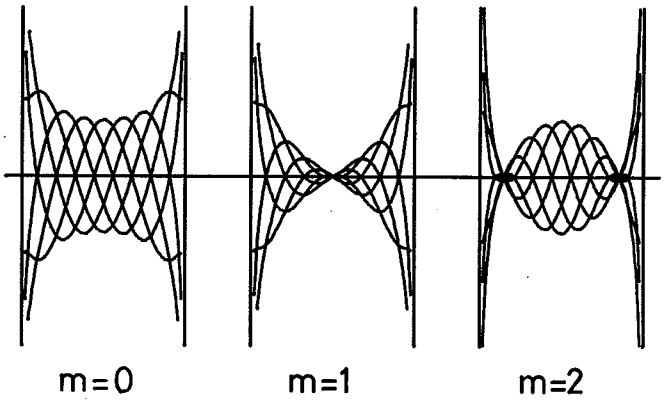

Fig. 3 Hollow-bunch modes for the same parameters as in Fig. 1c

Coupling impedance

Longitudinal

$$Z_{\parallel} = \frac{2\pi R}{2\pi b}\mathcal{R}_{surf} \qquad (6)$$

where $2\pi R$ = machine circumference, b = vacuum chamber radius, and $\mathcal{R}_{surf}$ is the surface impedance in ohms per square. In this case the beam sees a uniform longitudinal electric field set up by the return currents flowing in the vacuum chamber walls.

Transverse

The wall currents flow in opposite directions on either side of the vacuum chamber (or whatever is enclosing the beam) and set up a transverse magnetic field and a longitudinal electric field that varies in strength across the aperture (Fig. 4). Energy extracted from the directed motion of the beam by the longitudinal electric field drives the wall currents, which set up the dipole magnetic field, which deflects the beam. Expressed in equations, the power lost per unit length by the beam is

$$\int E\cdot J\, dx\, dy = -\frac{E_0}{b}\Delta \int y \frac{\partial J_0}{\partial y}\, dx\, dy \qquad (7)$$

$$= \frac{E_0\Delta}{b} I$$

while the power flow into the walls is $-2I_w E_0$, and therefore

$$I_w = -\frac{1}{2}\frac{\Delta}{b} I \, . \qquad (8)$$

This current is related to the electric field at the wall by the wall impedance,

$$E_0 = 4\frac{I_w Z_{\parallel}}{2\pi R} \, , \qquad (9)$$

where in place of the actual current distribution in the wall, we assume that I_w is confined within a strip of width $\frac{1}{4}$ the pipe circumference. This gives the correct result for a circular pipe, which has a cos θ current distribution. The deflecting magnetic field is (from Fig. 4)

$$B_x = -j\frac{2\Delta}{\omega b^2}\frac{Z_{\parallel} I}{2\pi R} e^{j\omega t} \, , \qquad (10)$$

and when this is inserted into the definition

$$Z_{\perp} = j\frac{\int_0^{2\pi R}\left[E + v\times B\right]_{\perp} ds}{\beta I \Delta} \, , \qquad \text{(ohms/metre)} \qquad (11)$$

one finds

$$Z_{\perp} = \frac{2c}{b^2}\frac{Z_{\parallel}}{\omega} \, , \qquad (12)$$

where c is the speed of light (3×10^8 m/sec) and $\beta = v/c$. The definition (11) was introduced by Hereward, and is used extensively by the ISR group.

The convenient relation (12) between $Z_{\perp}(\omega)$ and $Z_{\parallel}(\omega)$ is strictly valid for a round pipe with surface impedance $\mathcal{R}_{surf}$ and for frequencies sufficiently below cut-off that the fields have the simple form shown in Fig. 4. On the other hand, for perfectly conducting walls ($\mathcal{R}_{surf} = 0$)

$$Z_{\perp} = -j\frac{RZ_0}{\beta^2\gamma^2}\left(\frac{1}{a^2} - \frac{1}{b^2}\right) \, , \qquad (13)$$

where $Z_0 = 377$ ohms, a = beam radius, and b = pipe radius. The additional contribution due to wall resistivity can be found from (6) and (12) with

$$\mathcal{R}_{surf} = (1 + j)\frac{\rho}{\delta} \qquad \text{(thick-wall)} \, , \qquad (14)$$

where ρ is the resistivity (ohm-m) and δ is the skin depth, which is assumed to be smaller than the wall thickness. At low frequencies where δ > wall thickness ℓ,

$$\mathcal{R}_{surf} = \frac{\rho}{\ell} \qquad \text{(thin-wall)} \qquad (15)$$

provided the impedance of the outside material (air, magnets, etc.) is sufficiently high that all currents

Fig. 4

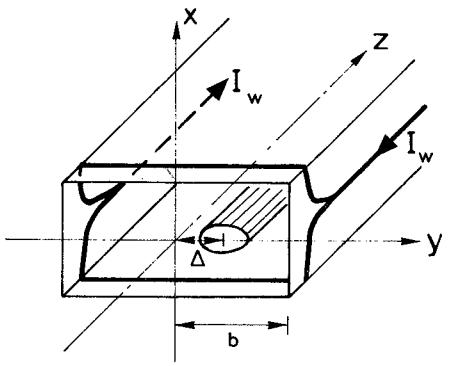

Currents:

I_w = wall current

$J_0(x,y-\Delta e^{j\omega t},z)$ = beam current density

$$\simeq J_0(x,y,z) - \frac{\partial J_0}{\partial y}\Delta e^{j\omega t}$$

with I = beam current = $\int J_0(x,y,z)\, dx\, dy$.

Fields:

$$E_z = E_0\frac{y}{b}e^{j\omega t} \qquad \text{(median plane)}$$

$$B_x = \frac{j}{\omega}\frac{E_0}{b}e^{j\omega t} \qquad (\text{from } \nabla\times E + \dot{B} = 0) \, .$$

flow through the walls. At low frequencies, $Z_\parallel$ is just the d.c. resistance of the vacuum chamber, typically about one ohm for stainless steel, and increases with frequency as $\sqrt{\omega}$ owing to the skin effect. Interruptions in the conducting vacuum chamber for ceramic or ferrite sections leads to much larger impedances. More elaborate and accurate calculations of $Z_\parallel$ and $Z_\perp$ or equivalently U and V can be found elsewhere[7-10], but the above approach is often sufficient.

Growth-rates in the absence of frequency spreads

The growth-rate is

$$\frac{1}{\tau} = -\mathrm{Im}\ \Delta\omega \qquad (16)$$

and the motion is unstable if Im $\Delta\omega$ is negative. For purpose of comparison, the coasting-beam growth-rate is found from

$$\Delta\omega = \frac{j}{2\omega_\beta}\frac{e\beta}{\gamma m_0}\frac{Z_\perp(\omega)I}{2\pi R} \qquad \text{(coasting beam)} \qquad (17)$$

$$= U + (1 - j)V$$

with $\omega = (n + Q)\omega_0 + \Delta\omega$ for the mode with $|n|$ wavelengths around the machine circumference $2\pi R$, beam current I, particle rest mass m_0, $\beta = v/c$, and $\omega_\beta = Q\omega_0$. MKS units are used throughout with an assumed time dependence exp (jωt). To compare with papers using exp (-iωt), replace j with -i in all formula.

For a bunched beam, the growth-rate involves a sum over the bunch spectrum. We need

$$h_m(\omega) = |\tilde{p}_m(\omega)|^2$$

where $\tilde{p}_m(\omega)$ is the Fourier transform of $p_m(t)$ (see Fig. 5). The spectrum is discrete with lines at $\omega_p = (p + Q)\omega_0$, $-\infty < p < \infty$ for a single bunch or several bunches oscillating independently. For coupled motion of M bunches, only every M^{th} line occurs with $p = n + kM$, $-\infty < k < \infty$, where n is the coupled-bunch mode number. It specifies the phase difference $2\pi|n|/M$ between adjacent bunches.

The growth-rate for mode m is found from

$$\Delta\omega_m = \frac{1}{1+m}\frac{j}{2\omega_\beta}\frac{e\beta}{\gamma m_0}\frac{I_0}{L}\frac{\sum_p Z_\perp(\omega_p)h_m(\omega_p-\omega_\xi)}{\sum_p h_m(\omega_p-\omega_\xi)}, \qquad (18)$$

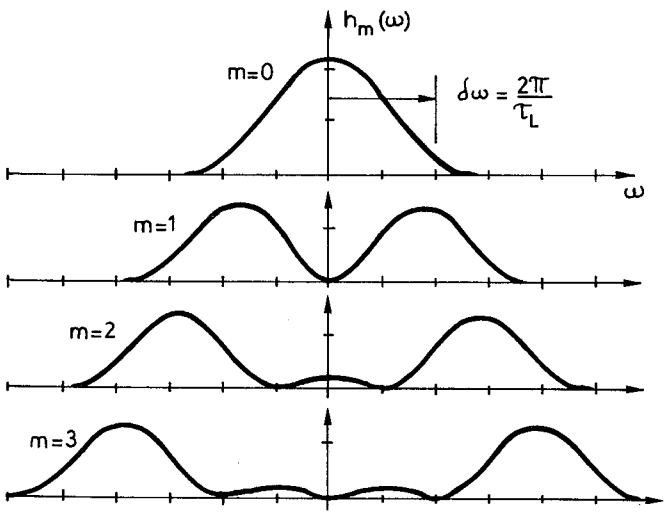

Fig. 5 Frequency spectrum for modes 0 to 3 with $\chi = 0$.

where I_0 is the current in one bunch of length L metres. The factor $(1 + m)^{-1}$ arises because the motion for the higher-order modes is constrained more and more to the few particles with large synchrotron amplitudes; this factor is absent for the hollow-bunch. Equation (18) is the general result. In the limit of short-range fields or smoothly varying $Z_\perp(\omega)$, it reduces to the classic head-tail effect, while in the opposite limit of long-range fields or rapidly varying $Z_\perp(\omega)$, it gives the multiturn contribution.

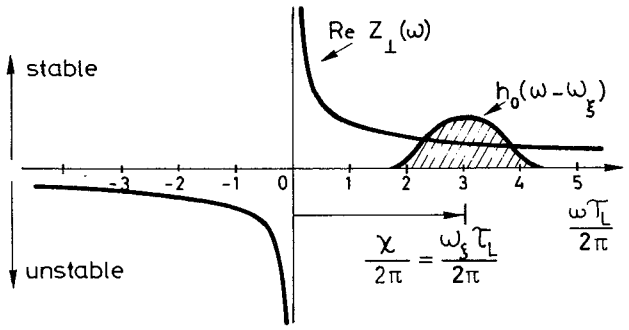

Fig. 6

As an example, consider Fig. 6, which is drawn for a positive phase shift χ so one is above transition with $\xi > 0$ or below transition with $\xi < 0$. The phase shift $\chi = 3 \times 2\pi$ corresponds to three oscillations along the bunch. Only the resistive or real part of $Z_\perp(\omega)$ causes instabilities, and this is drawn for a resistive-wall type impedance. Regardless of the type of impedance, the resistive part of $Z_\perp$ is positive for positive frequencies and negative for negative frequencies [from Eq. (12)]. From the figure, one sees that mode m = 0 is stable for χ positive and unstable for χ negative, and that this is true for any type of impedance.

If $Z_\perp(\omega)$ is sufficiently smooth that the sum in (18) can be replaced by an integration (discrete spectrum replaced by continuous spectrum), the growth-rate is independent of betatron frequency. In fact, the impedance shown is sufficiently smooth that it can be removed from the sum, and we find

$$\Delta\omega_0 = \frac{j}{2\omega_\beta}\frac{e\beta}{\gamma m_0}\frac{Z_\perp(\omega_\xi)I}{2\pi RB} \qquad (19)$$

which is just the coasting beam result (17) for the frequency ω_ξ with a bunching factor included ($B = ML/2\pi R$; $I = MI_0$).

It is convenient to rewrite (18) as

$$\Delta\omega_m = \frac{1}{1+m}\frac{e\beta I}{2\omega_\beta\ \gamma m_0\ 2\pi R}\times \qquad (20)$$

$$\left[\underbrace{\frac{1}{B}\frac{\int_{-\infty}^{\infty} Z_\perp(\omega)h_m(\omega-\omega_\xi)\,d\omega}{\int_{-\infty}^{\infty} h_m(\omega)\,d\omega}}_{\text{near field, independent of Q, } \to 0 \text{ or } \xi \to 0} + \underbrace{Z_\perp(\omega_n)F'_m(\chi-\omega_n\tau_L)}_{\text{multiturn fields, depend on Q, multiply by 1/M for independent bunch motion}}\right]$$

with the slowly varying part of $Z_\perp(\omega)$ separated from the rapidly varying part, where only one or a few lines $\omega_n = (n + Q)\omega_0$ contribute. The form factor $F'_m(\chi)$ is plotted in Fig. 7.

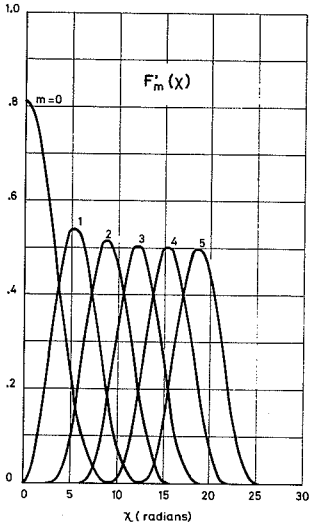

Fig. 7

If only a single line is important as for the narrow spectrum shown in Fig. 8, Eq. (20) again leads to the coasting beam result (17), but reduced by the factors F'_m and $(1 + m)^{-1}$.

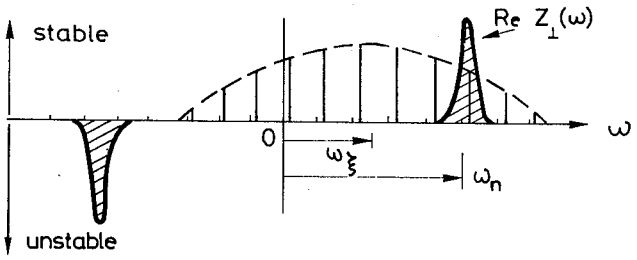

Fig. 8

A less obvious case is the resistive-wall impedance shown in Fig. 9, but here also only a single line contributes strongly to the long-range wake, namely the line $\omega_n = (n + Q)\omega_0$ nearest the origin. One easily recovers the usual rule that the mode number $|n|$ just above Q grows fastest. In the limit $\xi \to 0$ and for the thick-wall impedance (14), the multiturn part of (20) reduces to the familiar Courant and Sessler formula[3] (as corrected by Morton[11,12]). However, ξ is rarely zero, and often the frequency $|n-Q|\omega_0$ is sufficiently small that the thin-wall impedance (15) applies with consequently larger growth-rates. Although Fig. 9 is drawn for mode 0, for large enough χ the spectrum of

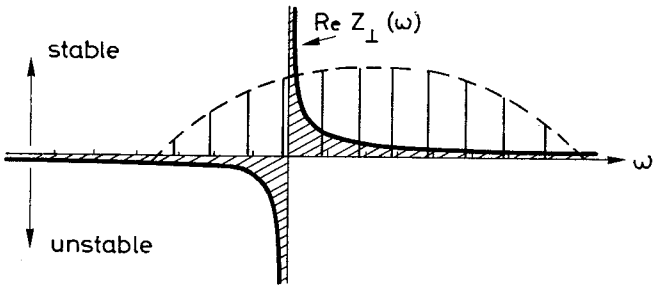

Fig. 9 The frequencies $\omega_n = (n + Q)\omega_0$ drawn for mode m = 0 and Q just below an integer

mode m overlaps the high impedance region near the origin: for example for χ = 9 radians, mode m = 2 grows fastest (see Figs. 1c and 7).

Now consider only the near-field part of (20). As an illustration of the graphical approach, the growth-rates of modes 0 and 2 for a resistive-wall impedance are sketched in Fig. 10b. As pointed out above, mode 0 is stable for positive χ, but one sees that mode 2 is unstable for small positive χ, and the reason is evident

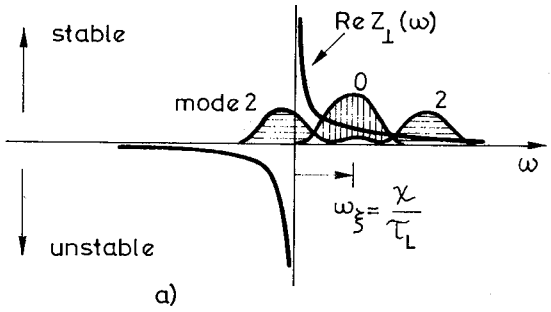

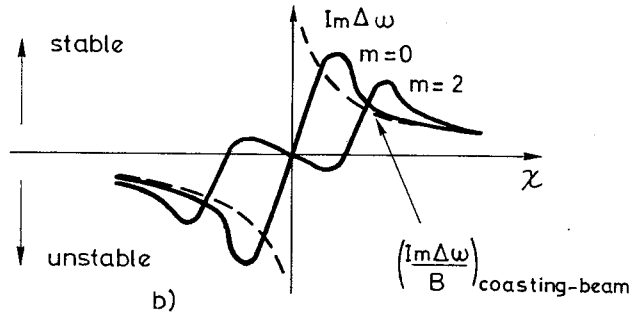

Fig. 10

from Fig. 10a. For χ sufficiently large, both modes have the same stability character as the coasting beam. The exact result for the thick-wall impedance (14) and sinusoidal modes is shown in Fig. 11, and the growth-rate is found from

$$\Delta\omega_m = \frac{j}{1+m}\,\frac{e\beta I}{2\omega_\beta\,\gamma m_0\,2\pi R}\times \qquad (21)$$

$$\times\left[\sqrt{\frac{2\pi}{MB}}\,Z_\perp(\omega_0)F_m(\chi) + Z_\perp(\omega_n)F'_m(\chi-\omega_n\tau_L)\right].$$

At this point some history is in order. The formula of Pellegrini[1] and Sands[2] is just the near-field part of (20), but expressed in the time domain and written explicitly for the hollow-bunch modes (5) and the resistive-wall impedance (14). They simplified the integration by considering only small χ, and found that the modes with m > 0 are unstable when mode 0 is stable, and vice versa. Later Zotter[13] carried out the integration numerically and found results similar to Fig. 11. However, the resistive-wall impedance is not sufficient to explain the fast growth-rates or absence of higher-order modes in electron storage rings. This is also true for the PS: Gareyte[6] has made detailed measurements of growth-rate as a function of phase-shift χ and has deduced from (19) that above 100 MHz the impedance rises slowly with frequency to a broad maximum around 1 GHz. Such an impedance can result from the several metres of ceramic and ferrite elements required for extraction magnets[9]. A slowly rising impedance also explains the absence of higher-order modes: from

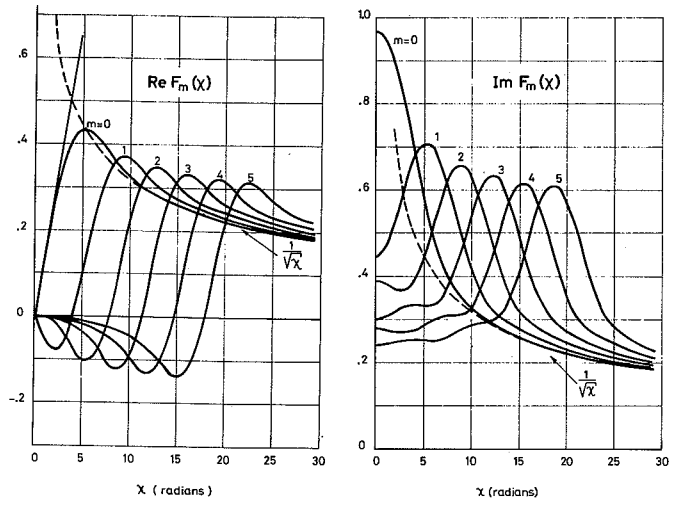

Fig. 11

Fig. 12 one sees that in this case the broad positive part of the spectrum contributes more than the narrow region of negative frequencies near the origin. This was also pointed out by Ruggiero[14]. One should have no trouble imagining other types of impedance and estimating the corresponding growth-rates.

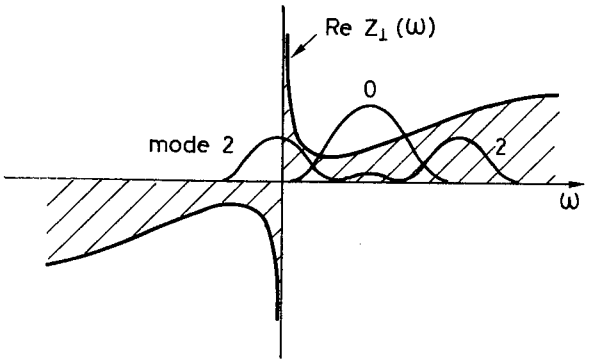

Fig. 12

Stability criterion

A sufficient spread in bunch frequencies prevents the coupled-bunch type instability. Such a spread may arise from a difference ΔN in bunch populations, via the coherent Laslett frequency shift $\Delta\omega_c = \Delta Q_c \omega_0$. For decoupled motion, the r.m.s. spread in bunch frequencies should exceed the growth-rate[12]

$$|\Delta\omega_c| \left(\frac{\Delta N}{N}\right)_{rms} > |\tau^{-1}| \ , \qquad (22)$$

and this may occur for large space-charge forces.

Octupoles cure either single-bunch or coupled-bunch instability if they produce enough frequency spread within a bunch to prevent its coherent motion, that is provided the spread in betatron frequencies exceeds the frequency shift $\Delta\omega_m$,

$$|\text{full-spread at half-height of } Q\omega_0| > |\Delta\omega_m| \ . \qquad (23)$$

Sextupoles or changes in machine chromaticity change the phase-shift χ, but do not contribute to Landau damping. For the long-range resistive-wall instability observed in the PS Booster, increasing χ shifts the instability to higher-order modes which have slower growth-rates. The opposite occurs for the PS or electron storage rings, namely the growth-rate increases as χ is made more negative.

Acknowledgements

I have profited very much from discussions with J. Gareyte, H.G. Hereward, K. Hübner, D. Möhl, and B. Zotter.

References

1. C. Pellegrini, Nuovo Cimento 64A, 477 (1969).
2. M. Sands, SLAC-TN-69/8 and 69/10.
3. E.D. Courant and A.M. Sessler, Rev. Sci. Instr. 37, 1579 (1966).
4. F.J. Sacherer, Methods for computing bunched-beam instabilities, CERN/SI BR/72-5.
5. F.J. Sacherer, Dispersion relations for head-tail modes, CERN/BR/74-4.
6. J. Gareyte and F. Sacherer, Head-tail type instabilities in the PS and Booster, these proceedings.
7. B. Zotter, CERN 69-15, CERN 69-16, CERN/ISR-TH/70-52, CERN/ISR-TH/71-13, and Particle Accelerators 1, 311 (1970).
8. R.J. Briggs and V.K. Neil, Plasma Physics 8, 255 (1966).
9. D. Möhl, Equipment responsible for transverse beam instability in the PS, CERN MPS/DL/Note 74-6.
10. L.J. Laslett, V.K. Neil and A.M. Sessler, Rev. Sci. Instr. 36, 436 (1965).
11. P.L. Morton, An investigation of space-charge effects for the booster injector to the CPS, CERN SI/Int. DL/68-3.
12. F.J. Sacherer, Spring Study on Accelerator Theory, 1972, Report to the 300 GeV Advisory Machine Committee, CERN, p. 159.
13. B. Zotter, The head-tail effect in the ISR, CERN-ISR-TH/69-60.
14. A.G. Ruggiero, The head-tail effect enhanced by a fast oscillating or fast decaying wake field, NAL report FN-254 (1973).